Conserved methionine dictates substrate preference in Nramp-family divalent metal transporters

Aaron T. Bozzi[a,1], Lukas B. Bane[a,1], Wilhelm A. Weihofen[a,2], Anne L. McCabe[a,3], Abhishek Singharoy[b], Christophe J. Chipot[c,d], Klaus Schulten[b,d], and Rachelle Gaudet[a,4]

[a]Department of Molecular and Cellular Biology, Harvard University, Cambridge, MA 02138; [b]Beckman Institute for Advanced Science and Technology, University of Illinois at Urbana–Champaign, Urbana, IL 61801; [c]Laboratoire International Associé Centre National de la Recherche Scientifique et University of Illinois at Urbana–Champaign, Unité Mixte de Recherche CNRS n°7565, Université de Lorraine, 54506 Vandoeuvre-lès-Nancy cedex, France; and [d]Department of Physics, University of Illinois at Urbana–Champaign, Urbana, IL 61801

Edited by Christopher Miller, Howard Hughes Medical Institute, Brandeis University, Waltham, MA, and approved July 21, 2016 (received for review May 25, 2016)

Natural resistance-associated macrophage protein (Nramp) family transporters catalyze uptake of essential divalent transition metals like iron and manganese. To discriminate against abundant competitors, the Nramp metal-binding site should favor softer transition metals, which interact either covalently or ionically with coordinating molecules, over hard calcium and magnesium, which interact mainly ionically. The metal-binding site contains an unusual, but conserved, methionine, and its sulfur coordinates transition metal substrates, suggesting a vital role in their transport. Using a bacterial Nramp model system, we show that, surprisingly, this conserved methionine is dispensable for transport of the physiological manganese substrate and similar divalents iron and cobalt, with several small amino acid replacements still enabling robust uptake. Moreover, the methionine sulfur's presence makes the toxic metal cadmium a preferred substrate. However, a methionine-to-alanine substitution enables transport of calcium and magnesium. Thus, the putative evolutionary pressure to maintain the Nramp metal-binding methionine likely exists because it—more effectively than any other amino acid—increases selectivity for low-abundance transition metal transport in the presence of high-abundance divalents like calcium and magnesium.

transition metals | MntH | divalent metal transporter DMT1 | hard-soft acid-base theory | ion selectivity filters

All organisms require transition metal ions as cofactors in proteins that perform a variety of essential cellular tasks. Through evolution, organisms have developed mechanisms to acquire, transport, and safely store essential metals such as manganese, iron, cobalt, and zinc. The natural resistance-associated macrophage protein (Nramp) family of metal transporters represents a common transition metal acquisition strategy conserved across all kingdoms of life (1). The first discovered mammalian Nramp (Nramp1) is expressed in phagosomal membranes and likely extracts essential metals to help kill engulfed pathogens (2, 3). Mammals use Nramp2, an essential gene also called DMT1, to absorb dietary iron into the enterocytes that line the small intestine (4) and to extract iron from transferrin-containing endosomes in all tissues. Bacteria express their own Nramp homologs, which they typically use to scavenge manganese and other first row divalent transition metals (5, 6). Last, most plants have several Nramp homologs that take up iron and manganese, the essential cofactor in photosystem II, from the soil or vacuolar stores (7, 8).

Nramps are generally thought to function as metal-proton symporters (1) and are able to bind and/or transport a wide range of divalent transition metal substrates, including the biologically useful metals Mn^{2+}, Fe^{2+}, Co^{2+}, Ni^{2+}, Cu^{2+}, and Zn^{2+}, as well as the toxic heavy metals Cd^{2+}, Pb^{2+}, and Hg^{2+} (4, 9–13). Nramps do discriminate against the divalent alkaline earth metal ions Mg^{2+} and Ca^{2+} (9, 14), which are typically several orders of magnitude more abundant than the transition metals (15). Using a bacterial Nramp homolog, *Deinococcus radiodurans* MntH, we demonstrate the role of the conserved metal-binding site methionine in conferring specificity against Ca^{2+} and Mg^{2+}, thus explaining at the molecular level the metal selectivity of Nramps.

Results

Conserved Metal-Binding Site Methionine Is Not Required for Transition Metal Transport. To validate *Deinococcus radiodurans* MntH (DraNramp) as a model system, we developed a cell-based cobalt uptake assay adapted from a similar assay in yeast (16). In this colorimetric assay, we quantify the relative Co^{2+} accumulation in Nramp-expressing *E. coli* at various time points by precipitating the transported Co^{2+} to the black solid cobalt (II) sulfide (Fig. S1*A*). We observed time-dependent Co^{2+} uptake for DraNramp, *Escherichia coli* MntH (EcoNramp), and *Staphylococcus capitis* MntH (ScaNramp) (Fig. S1*B*), which roughly correlated with expression levels of these His-tagged proteins (Fig. S1*C*).

In the inward-facing conformational state revealed by the ScaNramp crystal structures, three conserved side chains and a backbone carbonyl group formed the coordination sphere of bound transition metals (9). In DraNramp, these correspond to D56, N59, M230, and the backbone carbonyl of A227 (Fig. 1 *A*

Significance

Transition metals are micronutrients that all organisms use in essential metabolic processes. The ubiquitous Natural resistance-associated macrophage protein (Nramp) family facilitates the acquisition of these metal ions by transporting them across cellular membranes, including dietary iron absorption in mammals. We show that a conserved methionine, an unusual metal-binding residue found in the Nramp metal-binding site, is not essential for the transport of physiological environmentally scarce transition metals like iron and manganese. Instead, it confers selectivity against the abundant alkaline earth metals calcium and magnesium, with the tradeoff of making the toxic metal cadmium a preferred substrate. Using protein structure information, biochemical results, molecular dynamics simulations, and inorganic chemistry theory, we propose a model for how metal discrimination is enforced.

Author contributions: A.T.B., L.B.B., W.A.W., A.S., C.J.C., K.S., and R.G. designed research; A.T.B., L.B.B., and A.S. performed research; W.A.W. and A.L.M. contributed new reagents/analytic tools; A.T.B., L.B.B., A.S., C.J.C., and R.G. analyzed data; and A.T.B., L.B.B., A.S., C.J.C., and R.G. wrote the paper.

The authors declare no conflict of interest.

This article is a PNAS Direct Submission.

[1]A.T.B. and L.B.B. contributed equally to this work.

[2]Present address: Novartis Institutes for Biomedical Research, Cambridge, MA 02139.

[3]Present address: Department of Molecular Biology, Princeton University, Princeton, NJ 08544.

[4]To whom correspondence should be addressed. Email: gaudet@mcb.harvard.edu.

This article contains supporting information online at www.pnas.org/lookup/suppl/doi:10.1073/pnas.1607734113/-/DCSupplemental.

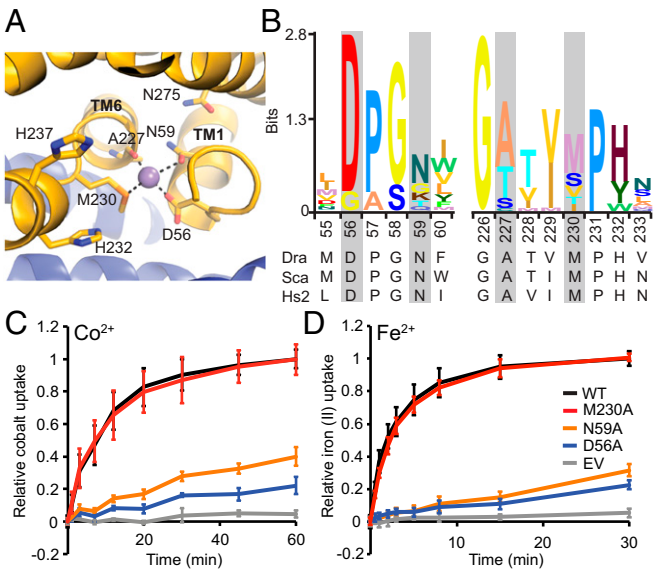

Fig. 1. The conserved metal-binding site methionine is not required for transport Co^{2+} and Fe^{2+}. (*A*) The ScaNramp structure identified four residues that directly bind metal substrate as D56, N59, A227, and M230 (DraNramp numbering). (*B*) Sequence logo of metal-binding site from 2,691 related sequences. Alignment was generated using HMMER with the DraNramp sequence as the search sequence within the UniprotRef database, with an E-value cutoff of 1×10^{-9}. Metal-coordinating residues are identified by gray rectangles. (*C*) In vivo Co^{2+} transport was greatly reduced for D56A and N59A compared with WT DraNramp, but M230A retained full activity. (*D*) Phenotypes for in vivo Fe^{2+} uptake were similar to Co^{2+}. Error bars are SDs ($n = 4$).

and *B*). The conserved methionine in the metal-binding site was postulated to stabilize transition metal substrates, facilitating their transport (9). To better understand the roles of the three metal-coordinating side chains, we mutated each residue to alanine and measured Co^{2+} transport by the resulting DraNramp variants (Fig. 1*C*). Loss of a metal-coordinating residue that uses oxygen to bind the metal, D56 or N59, was detrimental to Co^{2+} uptake, consistent with the previously demonstrated importance of these residues to the transport of Co^{2+}, Fe^{2+}, Mn^{2+}, and Cd^{2+} in bacterial and eukaryotic Nramp homologs (9, 17–20).

In stark contrast to D56A and N59A, M230A, which lacks the metal-binding thioether sulfur, transported Co^{2+} at rates and levels similar to WT DraNramp. We also observed this unexpected mutant phenotype with another essential metal, as M230A and WT transported Fe^{2+} similarly, whereas D56A and N59A were both severely impaired (Fig. 1*D* and Fig. S1*D*).

To test the generality of this robust transport activity of the M-to-A mutant, we used Fura-2 fluorescence to measure metal transport by HEK cells expressing WT human Nramp2 or binding-site mutants D86A and M265A. WT Nramp2 enabled Fe^{2+} and Co^{2+} transport (Fig. 2*A* and Fig. S2*A*), in agreement with our DraNramp results, as well as Mn^{2+} and Cd^{2+} (Fig. S2*B* and Fig. S2*C*), but not Ca^{2+} (Fig. S2*D*), consistent with previous studies with mammalian Nramp2 homologs (9, 11, 14, 21). However, in contrast to DraNramp M230A, M265A did not transport any of the tested metals, similarly to the D86A loss-of-function phenotype, even though both variants expressed as well as WT (Fig. S2*E*).

To determine whether DraNramp represented an evolutionary outlier, we tested Fe^{2+} transport by a variety of bacterial Nramps and their corresponding M-to-A and D-to-A mutants, expressed in *E. coli* (Fig. 2 *B* and *C* and Fig. S3). Like DraNramp, the *E. coli*, *Salmonella typhimurium*, *Klebsiella pneumonia*, *Serratia marcescens*, *Pseudomonas aeruginosa*, and *Xanthomonas campestris* M-to-A mutants exhibited similar or enhanced Fe^{2+} transport relative to their WT counterpart. In contrast, the *S. capitis, Staphylococcus aureus*, *Streptococcus mutans*, and *Deinococcus maricopensis* M-to-A mutants showed significantly impaired Fe^{2+} transport. The M-to-A mutation phenotype does not cluster in the phylogenetic tree; members of two distinct evolutionary clades of Nramps tolerate an M-to-A substitution for Fe^{2+} transport (Fig. S4) (22, 23). Thus, the observed differences are unlikely due to a broad mechanistic divergence within the Nramp family, and instead likely depend on sequence and structure context. We therefore decided to use DraNramp and its transport-competent methionine-less mutant to test the hypothesis that a primary role of this methionine is to specifically discriminate against binding or transport of certain metals.

The Methionine Reduces Alkaline Earth Metal Competition. To test our metal-discrimination hypothesis, we compared Co^{2+} transport by WT DraNramp and M230A in the presence of various concentrations of competing Mg^{2+}, Ca^{2+}, Mn^{2+}, Zn^{2+}, and Cd^{2+}, none of which form dark sulfide salts, and determined IC_{50} values for their inhibition of Nramp-dependent Co^{2+} transport (Fig. 3). Consistent with our hypothesis, both alkaline earth metals Mg^{2+} and Ca^{2+} inhibited Co^{2+} transport by M230A more effectively relative to WT (Fig. 3 *C* and *D* and Fig. S5*B*). In contrast, the first row transition metals Mn^{2+} (the physiological substrate) and Zn^{2+}, as well as the second row transition metal Cd^{2+}, competed Co^{2+} transport more effectively in WT relative to M230A (Fig. 3 *A*, *B*, and *D* and Fig. S5*A*). For most tested metals, this assay cannot discriminate between simple inhibition of cobalt transport or uptake of the competing metal, as their sulfide salts are white (MgS, CaS, ZnS) or light brown (MnS). However, WT DraNramp-expressing cells exposed to equal concentrations of Cd^{2+} and Co^{2+} turned yellow on $(NH_4)_2S$ addition, due to formation of the yellow solid cadmium (II) sulfide, whereas M230A cells remained black (Fig. S5*C*). Thus, WT DraNramp preferentially transports Cd^{2+} over Co^{2+}, whereas M230A preferentially transports Co^{2+} over Cd^{2+}. In summary, the metal-binding site methionine reduces the competition from the environmentally abundant Mg^{2+} and Ca^{2+} ions while also altering the relative substrate preferences among the rarer transition metals.

The Methionine Is Crucial for Both Promoting Cadmium and Reducing Calcium Transport. To directly test transport of additional metals, we reconstituted purified DraNramp into Fura-2-loaded proteoliposomes and monitored DraNramp-dependent transport over a range of Cd^{2+}, Mn^{2+}, or Ca^{2+} concentrations. Mn^{2+} quenches Fura-2 fluorescence at 340 nm, allowing relative influx measurements,

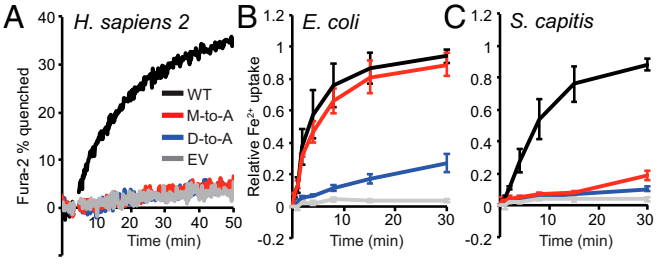

Fig. 2. The M-to-A mutation has species-specific effects on Nramp-dependent Fe^{2+} transport. (*A*) The M-to-A mutant in human Nramp2 does not transport Fe^{2+}. We monitored Fe^{2+} uptake in HEK 293 cells transfected with WT, D86A, or M265A HsNramp2, or an empty vector (EV), using Fura-2 quenching on binding Fe^{2+}. Traces are representative of observed metal uptake activity ($n = 3$). (*B* and *C*) The M-to-A mutation in the bacterial homologs EcoNramp (*B*) and ScaNramp (*C*) display starkly different phenotypes for Fe^{2+} transport when expressed in *E. coli*. Error bars are SD ($n = 3$). Mutants all expressed similarly to their respective WT (Figs. S2*E* and S3*B*).

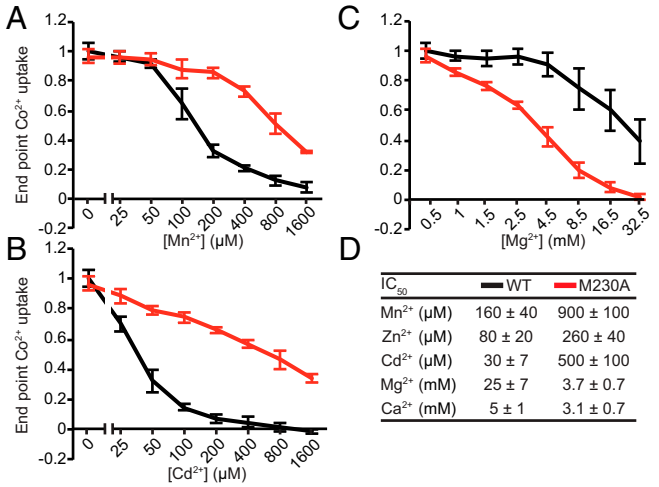

IC_{50}	WT	M230A
Mn^{2+} (μM)	160 ± 40	900 ± 100
Zn^{2+} (μM)	80 ± 20	260 ± 40
Cd^{2+} (μM)	30 ± 7	500 ± 100
Mg^{2+} (mM)	25 ± 7	3.7 ± 0.7
Ca^{2+} (mM)	5 ± 1	3.1 ± 0.7

Fig. 3. The metal-binding site methionine dictates DraNramp substrate competition against Co^{2+}. Uptake of 200 μM Co^{2+} by *E. coli* expressing either WT (black) or M230A (red) DraNramp was measured in the presence of varying concentrations of competing divalent metals. The transition metals Mn^{2+} (*A*), Cd^{2+} (*B*), and Zn^{2+} (Fig. S5*A*) compete more effectively for WT than for M230A DraNramp Co^{2+} transport. Conversely, the alkaline earth metals Mg^{2+} (*C*) and Ca^{2+} (Fig. S5*B*) compete more effectively for M230A than for WT DraNramp Co^{2+} transport. Error bars are SD ($n = 4$). (*D*) IC_{50} values with SE for added metals calculated for each metal, assuming a Hill coefficient of 1.

and we determined intraliposome Cd^{2+} or Ca^{2+} concentrations using ratiometric Fura-2 fluorescence (Fig. S6 *A–D*). Mn^{2+} was transported similarly by WT and M230A, whereas D56A showed little Mn^{2+} transport activity (Fig. 4*A*). In contrast, WT transported Cd^{2+} much more efficiently than either M230A or D56A (Fig. 4*B*), which demonstrates the importance of both residues to making Cd^{2+} a good substrate. Importantly, M230A transported Ca^{2+} more efficiently than either WT or D56A (Fig. 4*C*), showing how this methionine serves to deter Ca^{2+} transport. Our in vitro data suggest that the binding-site methionine is dispensable for transport of the biological substrate Mn^{2+}, consistent with our in vivo observations for the similar metals Co^{2+} and Fe^{2+}. However, the methionine is essential to both promote transport of the toxic metal Cd^{2+} and prevent transport of the alkaline earth metal Ca^{2+}. Of note, the D56A mutation impaired transport of all tested substrates, demonstrating the importance of the conserved aspartate to the general metal transport mechanism. In contrast, the M230A mutation retains transport function, although with altered metal transport preferences, suggesting the methionine functions as a selectivity filter.

To further investigate the underlying cause of the pronounced difference in Cd^{2+} transport by WT and M230A DraNramp, we measured the in vitro Cd^{2+}-binding affinity of these two proteins using microscale thermophoresis (Fig. 4 *D* and *E*). We used purified Strep-tagged protein that was Cy5-maleimide–labeled at a lone cysteine replacing R211 in extracellular loop 5–6; this R211C/C382S construct shows WT-like Co^{2+} transport activity and similar Cd^{2+} and Mg^{2+} competition phenotypes (Fig. S6*E*). WT protein bound Cd^{2+} with a K_D of 10.6 ± 3.6 μM, similar to the 29 ± 10 μM value determined for WT ScaNramp using ITC (9). In contrast, M230A showed no clear Cd^{2+}-binding signal. This result demonstrates the importance of M230 for Cd^{2+} binding in WT DraNramp and suggests that reduced binding affinity directly causes Cd^{2+} transport impairment in M230A. In contrast, we observed a similar trend in binding behavior of Mn^{2+} (which WT and M230A both transport) for WT and M230A (Fig. S6 *F* and *G*), although we did not calculate K_D values due to the higher noise in the data.

To extend these observations regarding the differential importance of the methionine to the transport of different metals, we performed a series of molecular dynamics simulations, which we discuss in depth in *SI Discussion*, using the available ScaNramp structure to compare how different ions equilibrate in and exit the conserved binding site (Fig. S7). These simulations showed that if an ion can interact favorably with the methionine, it experiences greater stabilization in the binding site and a lower-energy exit pathway in the intracellular conformation than an ion that cannot interact with the methionine.

Only the Native M230 Allows Transition Metal Transport in High Mg^{2+} Concentrations. To determine how the unique chemical properties of the binding-site methionine affect metal transport and selectivity, we used our in vivo assay to measure Co^{2+} and Fe^{2+} uptake by a panel of 20 DraNramp variants, with each possible amino acid substituted at position 230 (Fig. 5*A* and Fig. S8). The clear trend is that only small residues—glycine, alanine, serine, threonine, and cysteine—or the native methionine enabled efficient metal transport. This result suggests that other electron-donating functional groups can substitute for the thioether sulfur while preserving transition metal transport. For example, alanine or glycine could provide enough room for one or more water molecules to coordinate the metal (Fig. S8*A*). Similarly, the threonine or serine hydroxyl group may either directly bind the metal or help align a metal-binding water molecule, but the striking functional difference between the isosteric threonine and valine residues demonstrates the importance of this side chain hydroxyl. Additionally, little metal transport was observed when we replaced M230 with the sterically similar but purely aliphatic isoleucine or leucine side chain, emphasizing the importance of having an electron-pair donor at this position to stabilize the metal substrate. Interestingly, we observed little metal uptake with larger residues that do contain common metal-binding functional groups (asparagine, glutamine, histidine, aspartate, and glutamate). This result may reflect the inability for large polar side chains to optimally orient within the metal-binding site.

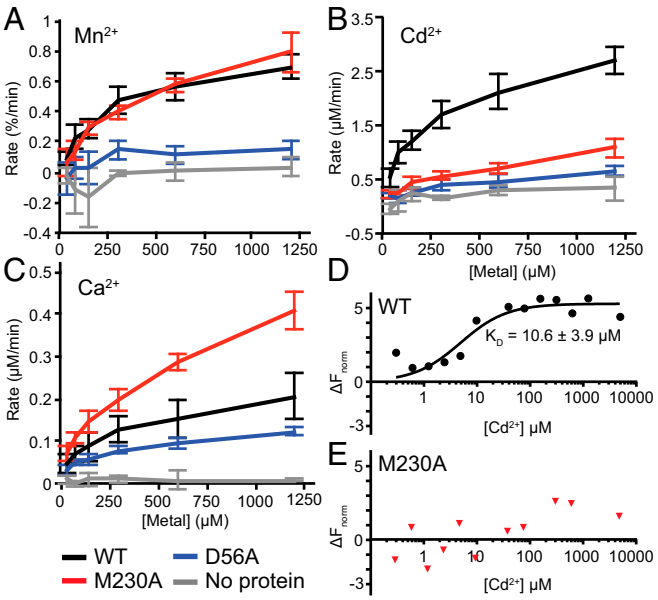

Fig. 4. In vitro transport and binding assays reveal M230's role in metal selectivity. (*A–C*) Initial transport rates for Mn^{2+} (*A*), Cd^{2+} (*B*), and Ca^{2+} (*C*) are shown for WT DraNramp (black), M230A (red), D56A (blue), and empty (no protein) liposomes (gray). Error bars are SD from $n = 3$ or 4. (*D* and *E*) Binding isotherms showing WT DraNramp (*D*) and M230A (*E*) affinity for Cd^{2+}. Representative data are shown ($n = 4$) and the error on K_D is SD.

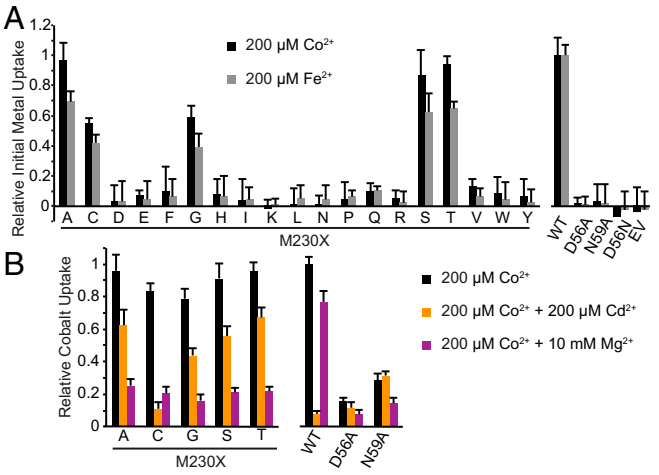

Fig. 5. Substitutions to small amino acids at position 230 retain metal transport ability. (*A*) Initial Co^{2+} (black bars, 5-min time point) and Fe^{2+} (gray bars, 1.5-min time point) transport levels measured for WT DraNramp or variants containing substitutions of M230 to each of the 19 other amino acids expressed in *E. coli* (Fig. S8*B*). We observed significant transport (relative to WT) of both metals with the small residues alanine, cysteine, glycine, serine, and threonine replacing M230. (*B*) Although several mutants transported Co^{2+} efficiently over the course of 60 min (black bars), only WT retains significant Co^{2+} transport with a moderate concentration of competing Mg^{2+} (magenta bars). However, only WT and M230C showed drastic reduction in Co^{2+} transport with an equal concentration of Cd^{2+} (gold bars). We used competing Mg^{2+} and Cd^{2+} concentrations showing significant differences between WT and M230A (Fig. 3). Error bars are SD ($n = 4$).

For WT DraNramp and the most active mutants, we measured end point Co^{2+} uptake in the absence or presence of the competing metals Cd^{2+} or Mg^{2+} (Fig. 5*B*). Strikingly, 10 mM Mg^{2+} inhibits all mutants, with only WT facilitating significant Co^{2+} transport. In contrast, 200 μM Cd^{2+} (1:1 ratio with Co^{2+}) severely reduced WT DraNramp Co^{2+} uptake, but did not impair the M230A, G, T, or S mutants to the same degree. Interestingly, Co^{2+} transport by M230C was inhibited by Cd^{2+} similarly to WT, which suggests the cysteine thiol group can directly coordinate the metal. Thus, the presence of a binding-site sulfur, whether from cysteine or methionine, is essential to making the toxic metal Cd^{2+} a preferred DraNramp substrate. In conclusion, although five small amino acid side chains can effectively replace the methionine to enable transition metal transport, only the native methionine offers robust selectivity in favor of transition metals in the presence of competing Mg^{2+}.

The Methionine Confers Tolerance to Ca^{2+} and Mg^{2+} While Facilitating Cd^{2+} Toxicity. To explore the biological relevance of metal selectivity, we determined the impact of different metal-binding site configurations on growth of DraNramp-expressing *E. coli* strains in the presence of various metals using a plate-based toxicity assay. We attribute impaired growth of Nramp-expressing *E. coli* to toxic intracellular accumulation of metal substrates. M230A- and D56A-expressing strains similarly tolerated Cd^{2+} at levels which prevented growth of WT-expressing cells (Fig. 6*A*), confirming the importance of both residues observed for Cd^{2+} uptake in liposomes. Likewise, Mn^{2+} inhibited growth of WT- and M230A-expressing strains at high micromolar concentrations that the D56A-expressing strains tolerated (Fig. 6*B*), which also echoes our liposome assay results. Interestingly, at low micromolar Mn^{2+} concentrations, M230A-expressing cells grew better than WT-expressing cells, which suggests that M230 is important for Mn^{2+} uptake at low concentrations and/or among competing alkaline earth metals (Ca^{2+} and Mg^{2+} are both present at hundreds of micromolar in LB agar) (24). Additionally, WT- and M230A-expressing cells were more susceptible to Zn^{2+}, and Fe^{2+} but not equivalent concentrations of Fe^{3+}, than their D56A counterparts (Fig. 6 *C* and *E*).

Notably, M230A-expressing cells fared worse at concentrations of Ca^{2+} or Mg^{2+} that WT-expressing cells tolerated (Fig. 6 *F* and *G*), supporting our Co^{2+} competition assay data. Interestingly, D56A-expressing cells grew noticeably less than WT-expressing cells at high Mg^{2+} or Ca^{2+} concentration, with a similar Ca^{2+}-mediated impairment as M230A. This result suggests that removing either of these two residues may allow nondiscriminatory metal inflow at high concentration gradients, with the intact binding site perhaps functioning as the principal metal transport gate. These metal toxicity observations were not unique to DraNramp, as EcoNramp-expressing cells likewise showed increased Cd^{2+}, decreased Ca^{2+}, and similar Mn^{2+} toxicity compared with the EcoNramp M-to-A mutant-expressing cells (Fig. S9). Overall, these metal toxicity assays provide indirect evidence of metal transport in a biological setting that largely corroborates our in vitro metal transport findings and emphasizes the importance of the methionine residue in selecting against the environmentally abundant Mg^{2+} and Ca^{2+}, but also increasing the ability to transport the toxic heavy metal Cd^{2+}.

Discussion

Our study demonstrates the role of the conserved metal-binding site methionine as the selectivity filter in Nramps. In contrast to the other binding site residues, it is not essential for transport of many biologically useful transition metals in DraNramp and several other homologs, although a mutation to alanine does slightly impair Mn^{2+} transport in some conditions. In addition, while this mutation drastically decreases transport of the toxic metal Cd^{2+}, it increases transport of Mg^{2+} and Ca^{2+}, which would likely be deleterious to most organisms.

Mutations of the binding site methionine have previously been investigated in a few species. In EcoNramp, an M-to-I or M-to-K mutation eliminated Mn^{2+} transport (25), which agrees with our lack of observed Fe^{2+} and Co^{2+} transport for those mutants in

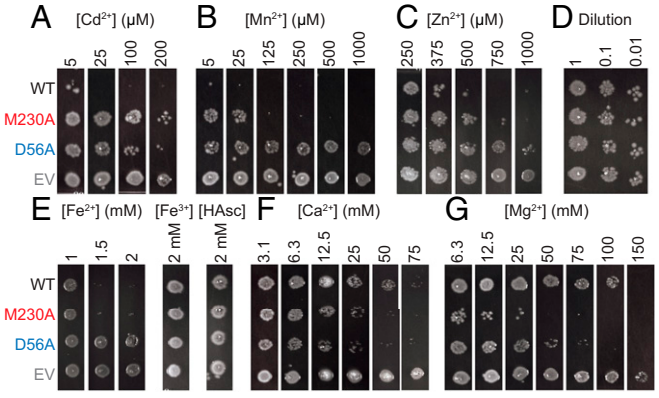

Fig. 6. Metal toxicity assays demonstrate the importance of M230 in filtering out abundant divalent metals. *E. coli* overexpressing either WT, M230A, or D56A DraNramp, or an empty vector control (EV) in liquid culture were spotted on LB agar containing indicated divalent metal concentrations, and grown overnight. (*A*) M230A- and D56A-expressing cells tolerated Cd^{2+} concentrations toxic to WT-expressing cells. (*B*) Low Mn^{2+} concentrations inhibited growth of WT-expressing cells, whereas M230A-expressing cells were inhibited at higher concentrations of Mn^{2+} that D56A-expressing cells tolerated. (*C*) Zn^{2+} inhibited cells expressing WT > M230A > D56A. (*D*) Control dilutions plated in the absence of added divalent metals. (*E*) Fe^{2+}, but not Fe^{3+}, inhibited growth of WT- and M230A-expressing cells equally, but not D56A-expressing cells. (*F*) WT-expressing cells grew on higher concentrations of Ca^{2+} than either M230A- or D56A-expressing cells. (*G*) WT-expressing cells tolerated much higher Mg^{2+} concentrations than their M230A, and to a lesser extent, D56A counterparts. Images representative of $n = 3$ results.

DraNramp. Consistent with our findings regarding the methionine's importance for Cd^{2+} binding and transport in DraNramp, an M-to-A mutation in ScaNramp significantly decreased Cd^{2+} binding affinity, and the analogous mutation in human Nramp2 reduced Cd^{2+} transport (9), a phenotype we replicated and extended by showing loss of Co^{2+}, Mn^{2+}, and Fe^{2+} transport. We discovered a range of relative Fe^{2+} transport abilities for M-to-A mutants in different bacterial homologs (Fig. 2 and Fig. S3) that stretched from no apparent activity for M226A ScaNramp to approximately WT-level transport in M230A DraNramp and M209A EcoNramp to enhanced transport in M236A *S. marcescens* Nramp.

Our DraNramp results suggest that the main purpose of Nramp's binding site methionine is to reduce Mg^{2+} and Ca^{2+} transport, thus avoiding their overaccumulation and preventing competition with the rarer transition metals that are Nramp's intended substrates. Inorganic chemistry theory helps explain how many proteins, including Nramp, evolved to discriminate among similar metal ions by tuning their binding-site chemical and structural properties. Interactions between metals and electron-donating ligands are typically strongest when either the ionic or covalent nature of the bond is maximized (26). Thus, highly electronegative ligands such as oxygen form strong bonds with "hard" metal ions like Mg^{2+}, which has a high charge in a small radius. Conversely, less electronegative, more polarizable ligands such as sulfur form the most stable bonds with "soft" metal ions like Cd^{2+}, which better share electron density in a covalent manner. In the empirical classification of metal ions as hard (favoring ionic interactions), intermediate (capable of both ionic and covalent interactions), or soft (favoring covalent interactions), Nramp's biological substrates—the first row transition metals—are considered intermediate, whereas Ca^{2+} and Mg^{2+} are hard, and Cd^{2+}, Pb^{2+}, and Hg^{2+} are soft. In Nramp's binding site, the soft methionine sulfur is the sole exception; all other metal-binding ligands are hard oxygens better suited to ionic bonds. The methionine therefore selectively stabilizes transition metals capable of covalent and semicovalent interactions.

Our data show that this methionine provides significant stabilization necessary for the binding and transport of Cd^{2+}, which like other soft toxic heavy metals can forge strong covalent-like interactions with sulfur. Additionally, our results suggest that the magnitude of the net methionine stabilization may be minimal for Nramp's biological substrates (the intermediate first row transition metals), whereas the ionic-interacting hard alkaline earth metals Ca^{2+} and Mg^{2+} (which become better substrates upon the methionine's removal) are effectively destabilized by its presence.

One potential explanation for the M-to-A mutant phenotype is that alanine enables substrate metal ions to retain one or more water ligands that they would otherwise shed upon coordination by the WT binding site. The M-to-A mutation would therefore both improve the binding environment for metals that prefer hard oxygen ligands (Mg^{2+} and Ca^{2+}) and impair the ability of a metal like Cd^{2+} that prefers soft ligands to bind while having only a minor effect on net affinity for intermediate metals that lack a strong preference between a hard and soft ligand. Our M-to-X substitution panel results support this model (Fig. 5): Small residues, which could leave free space for water, all enabled transport of intermediate metals Co^{2+} and Fe^{2+} while remaining susceptible to Mg^{2+} competition and decreasing Cd^{2+} preference (with the exception of the sulfur-containing cysteine), whereas larger residues such as leucine, which may not provide space for water, severely impaired transport.

Methionine is rarely found in binding sites for most metals, with the notable exception of copper (27, 28). However, the putative metal-binding site in the iron exporter ferroportin contains a methionine (29), suggesting a strategy similar to Nramps' for selective transition metal transport. Underscoring the methionine's key metal selectivity role, a functionally diverged Nramp-related transporter of the hard metal Al^{3+} in rice has a threonine (providing a hard oxygen ligand) in place of the methionine while retaining the other binding-site residues (30). Similarly the methionine is also replaced with threonine in two bacterial Nramp-related Mg^{2+} transporters (31). Intriguingly, Nramp homologs from several extremophilic prokyarotes that flourish in highly acidic and heavy metal rich environments (32) have an alanine in place of the methionine, suggesting this substitution is favored under the right selective pressure.

In this evolutionary context, Nramp's binding site methionine likely represents a tradeoff. We propose that this residue was selected and conserved primarily for its ability to deter competition from and transport of Ca^{2+} and Mg^{2+}, rather than for it being an optimal ligand for its intended substrates such as Mn^{2+} and Fe^{2+}. The alkaline earth metals are highly abundant in the environment (the ocean contains 50 mM Mg^{2+} and 10 mM Ca^{2+}) (33), and intracellular Ca^{2+} concentration is tightly regulated, with unchecked import disrupting cell viability, thus providing a strong selective pressure to guard against accidental transport. In addition, as the first row transition metals are approximately six orders of magnitude less abundant than the alkaline earth metals (33), organisms require a robust discrimatory mechanism to find those essential metals within a sea of Ca^{2+} and Mg^{2+}. However, the binding site methionine also serves as an optimal ligand for the toxic metal Cd^{2+}, enabling it to become an ideal substrate for Nramps: a detrimental property as Nramp activity has been linked to cadmium poisoning in mammals (34, 35). Nevertheless, the normally low environmental abundance of Cd^{2+} (two orders of magnitude below Mn^{2+}) likely did not provide significant selective pressure against the methionine on evolutionary time scales. In conclusion, our results explain the ability of Nramps to transport a variety of transition metals while highlighting the role of the conserved methionine in specifically discriminating against the abundant hard alkaline earth metals.

Methods

Additional methods are described in *SI Methods*.

DraNramp Microscale Thermophoresis Binding Assay. Purified strep-tagged fluorescently labeled DraNramps were diluted to 100 nM in 150 mM NaCl, 10 mM Hepes, pH 7.5, and 0.03% β-dodecylmaltoside (β-DDM), mixed 1:1 with 14 serially diluted $CdCl_2$ solutions, and loaded into Premium Coated capillaries (NanoTemper Technologies). Thermophoresis data were obtained with a NanoTemper Monolith NT.115 at 70% light-emitting diode, 80% microscale thermophoresis (MST) power and 30-s MST time, and analyzed using GraphPad prism.

DraNramp Reconstitution and Proteoliposome Activity Assays. Lipids [50:35:15 1-Palmitoyl-2-oleoyl-sn-glycero-3-phosphoethanolamine (POPE):1-Palmitoyl-2-oleoyl-sn-glycero-3-phosphocholine (POPC):1-Palmitoyl-2-oleoyl-sn-glycero-3-phospho-rac-glycerol (POPG); Avanti Polar Lipids] and freshly purified DraNramp at a 1:500 mass ratio and 5 mM β-decylmaltoside (β-DM) were dialyzed against 10 mM Mops, pH 7.0, and 100 mM KCl at 4 °C for 2–3 d and at room temperature for 1 d. After three freeze-thaw cycles to incorporate Fura-2 (100 μM), liposomes were extruded through a 400-nm filter, separated from bulk dye on a PD-10 column (GE Life Sciences), and diluted threefold into 10 mM Mops, pH 7.0, and 100 mM NaCl in a 96-well black clear-bottom assay plate (Greiner). After measuring baseline fluorescence for 5 min, metal substrate was added, along with 50 nM valinomycin to establish a negative internal potential. Fluorescence (λ_{ex} = 340 and 380 nm; λ_{em} = 510 nm) was monitored at room temperature for 70 min, adding ionomycin (0.25 μM) at 60 min to measure maximum signal. The intraliposome concentration of Cd^{2+} or Ca^{2+} was determined using $[M^{2+}]_{inside} = ([M^{2+}]_{free}[\text{Fura-2}]_{total})/(K_D + [M^{2+}]_{free}) + [M^{2+}]_{free}$, where K_D is for M^{2+} and Fura-2 (Cd^{2+} = 1 pM; Ca^{2+} = 135 nM) (36, 37). Transport rates were determined by linear regression of the data for the first 10 min after adding Cd^{2+} or 60 min after adding Mn^{2+} or Ca^{2+}.

In Vivo Metal Uptake Assays in *E. coli*. *E. coli* expressing bacterial Nramps at OD = 5.26 in 190 μL assay buffer [50 mM Hepes, pH 7.3, or 2-(*N*-morpholino) ethanesulfonic acid (Mes), pH 6.4, for Fig. 2 and Fig. S3 data, 60 mM NaCl, 10 mM KCl, 0.5 mM $MgCl_2$, and 0.217% glucose] were distributed into 96-well plates at 37 °C. To initiate uptake, 10 μL 20× metal solution [4 mM $Co(NO_3)_2$, 4 mM freshly made $FeSO_4$ in 4 mM ascorbic acid, or a mixture of 4 mM Co $(NO_3)_2$ with competing metal as chloride salt] was added. To quench uptake,

10 μL 100 mM EDTA (20 μL 200 mM EDTA when Ca^{2+} or Mg^{2+} was included) was added. Cells were pelleted and washed three times before precipitating the metal with 1% $(NH_4)_2S$. Scanned images of the resulting pellets were converted to black and white, and pellet darkness was determined using ImageJ64 (NIH).

In Vivo Metal Uptake Assays in HEK293 Cells. Fifty microliters of 150 mM NaCl, 4.5 mM KCl, 0.2 mM $MgCl_2$, 10 mM glucose, and 20 mM Mes, pH 5.5, was added to transfected Fura-2–loaded HEK293 cells. Fluorescence (λ_{ex} = 340 and 380 nm; λ_{em} = 510 nm) was monitored for a 2- to 4-min baseline and 45 min after adding 25 μL 3× metal solution [$Co(NO_3)_2$, $MnCl_2$, $CdCl_2$, $CaCl_2$, or $FeSO_4$ + ascorbic acid].

Metal Toxicity Assay. Isopropyl β-D-1-thiogalactopyranoside (IPTG)-induced *E. coli* expressing bacterial Nramps (1 μL of dilutions to OD_{600} = 0.01, 0.001, or 0.0001 in LB) were plated onto LB ampicillin agar containing various concentrations of added metal, and the plates were imaged using an AlphaImager system after overnight incubation at 37 °C. Gamma values were adjusted the same way for all images to increase contrast.

ACKNOWLEDGMENTS. We thank Ming-Feng Tsai, Chris Miller, and Ute Hellmich for assistance with developing the liposome assay; Ali Raja, Gunes Bozkurt, and Hao Wu for assistance with the microscale thermophoresis system; Jack Nicoludis and members of the R.G. laboratory for discussions; Mathieu Cellier for providing several bacterial Nramp clones; and Raimund Dutzler for sharing the ScaNramp coordinates before release and providing the ScaNramp gene. The work was funded in part by a Basil O'Connor Starter Scholar research award from the March of Dimes Foundation (to R.G.), NIH Grant 9P41GM104601 (to K.S.), and a Beckman Postdoctoral Fellowship (to A.S.). We gladly acknowledge supercomputer time from the Texas Advanced Computing Center via Extreme Science and Engineering Discovery Environment Grant National Science Foundation (NSF)-MCA93S028.

1. Courville P, Chaloupka R, Cellier MFM (2006) Recent progress in structure-function analyses of Nramp proton-dependent metal-ion transporters. *Biochem Cell Biol* 84(6): 960–978.
2. Cellier MF, Courville P, Campion C (2007) Nramp1 phagocyte intracellular metal withdrawal defense. *Microbes Infect* 9(14-15):1662–1670.
3. Vidal S, Belouchi AM, Cellier M, Beatty B, Gros P (1995) Cloning and characterization of a second human NRAMP gene on chromosome 12q13. *Mamm Genome* 6(4): 224–230.
4. Gunshin H, et al. (1997) Cloning and characterization of a mammalian proton-coupled metal-ion transporter. *Nature* 388(6641):482–488.
5. Agranoff D, Monahan IM, Mangan JA, Butcher PD, Krishna S (1999) Mycobacterium tuberculosis expresses a novel pH-dependent divalent cation transporter belonging to the Nramp family. *J Exp Med* 190(5):717–724.
6. Kehres DG, Zaharik ML, Finlay BB, Maguire ME (2000) The NRAMP proteins of Salmonella typhimurium and Escherichia coli are selective manganese transporters involved in the response to reactive oxygen. *Mol Microbiol* 36(5):1085–1100.
7. Cailliatte R, Schikora A, Briat JF, Mari S, Curie C (2010) High-affinity manganese uptake by the metal transporter NRAMP1 is essential for Arabidopsis growth in low manganese conditions. *Plant Cell* 22(3):904–917.
8. Colangelo EP, Guerinot ML (2006) Put the metal to the petal: Metal uptake and transport throughout plants. *Curr Opin Plant Biol* 9(3):322–330.
9. Ehrnstorfer IA, Geertsma ER, Pardon E, Steyaert J, Dutzler R (2014) Crystal structure of a SLC11 (NRAMP) transporter reveals the basis for transition-metal ion transport. *Nat Struct Mol Biol* 21(11):990–996.
10. Milner MJ, et al. (2014) Root and shoot transcriptome analysis of two ecotypes of Noccaea caerulescens uncovers the role of NcNramp1 in Cd hyperaccumulation. *Plant J* 78(3):398–410.
11. Picard V, Govoni G, Jabado N, Gros P (2000) Nramp 2 (DCT1/DMT1) expressed at the plasma membrane transports iron and other divalent cations into a calcein-accessible cytoplasmic pool. *J Biol Chem* 275(46):35738–35745.
12. Illing AC, Shawki A, Cunningham CL, Mackenzie B (2012) Substrate profile and metal-ion selectivity of human divalent metal-ion transporter-1. *J Biol Chem* 287(36): 30485–30496.
13. Vázquez M, Vélez D, Devesa V, Puig S (2015) Participation of divalent cation transporter DMT1 in the uptake of inorganic mercury. *Toxicology* 331:119–124.
14. Xu H, Jin J, DeFelice LJ, Andrews NC, Clapham DE (2004) A spontaneous, recurrent mutation in divalent metal transporter-1 exposes a calcium entry pathway. *PLoS Biol* 2(3):E50.
15. Cowan JA (1995) *The Biological Chemistry of Magnesium* (VCH, New York), p xvi.
16. Myers BR, Bohlen CJ, Julius D (2008) A yeast genetic screen reveals a critical role for the pore helix domain in TRP channel gating. *Neuron* 58(3):362–373.
17. Chaloupka R, et al. (2005) Identification of functional amino acids in the Nramp family by a combination of evolutionary analysis and biophysical studies of metal and proton cotransport in vivo. *Biochemistry* 44(2):726–733.
18. Courville P, et al. (2008) Solute carrier 11 cation symport requires distinct residues in transmembrane helices 1 and 6. *J Biol Chem* 283(15):9651–9658.
19. Haemig HAH, Brooker RJ (2004) Importance of conserved acidic residues in mntH, the Nramp homolog of Escherichia coli. *J Membr Biol* 201(2):97–107.
20. Lam-Yuk-Tseung S, Govoni G, Forbes J, Gros P (2003) Iron transport by Nramp2/DMT1: pH regulation of transport by 2 histidines in transmembrane domain 6. *Blood* 101(9): 3699–3707.
21. Forbes JR, Gros P (2003) Iron, manganese, and cobalt transport by Nramp1 (Slc11a1) and Nramp2 (Slc11a2) expressed at the plasma membrane. *Blood* 102(5):1884–1892.
22. Cellier MF, Bergevin I, Boyer E, Richer E (2001) Polyphyletic origins of bacterial Nramp transporters. *Trends Genet* 17(7):365–370.
23. Dereeper A, et al. (2008) Phylogeny.fr: Robust phylogenetic analysis for the non-specialist. *Nucl Acids Res* 36(Web Server Issue):W465–W469.
24. Abelovska L, et al. (2007) Comparison of element levels in minimal and complex yeast media. *Can J Microbiol* 53(4):533–535.
25. Haemig HAH, Moen PJ, Brooker RJ (2010) Evidence that highly conserved residues of transmembrane segment 6 of Escherichia coli MntH are important for transport activity. *Biochemistry* 49(22):4662–4671.
26. Pearson RG (1963) Hard and soft acids and bases. *J Am Chem Soc* 85(22):3533–3539.
27. Zheng H, Chruszcz M, Lasota P, Lebioda L, Minor W (2008) Data mining of metal ion environments present in protein structures. *J Inorg Biochem* 102(9):1765–1776.
28. Harding MM (2004) The architecture of metal coordination groups in proteins. *Acta Crystallogr D Biol Crystallogr* 60(Pt 5):849–859.
29. Taniguchi R, et al. (2015) Outward- and inward-facing structures of a putative bacterial transition-metal transporter with homology to ferroportin. *Nat Commun* 6: 8545.
30. Xia J, Yamaji N, Kasai T, Ma JF (2010) Plasma membrane-localized transporter for aluminum in rice. *Proc Natl Acad Sci USA* 107(43):18381–18385.
31. Shin JH, et al. (2014) Transport of magnesium by a bacterial Nramp-related gene. *PLoS Genet* 10(6):e1004429.
32. Mangold S, Potrykus J, Bjorn E, Lovgren L, Dopson M (2013) Extreme zinc tolerance in acidophilic microorganisms from the bacterial and archaeal domains. *Extremophiles* 17(1):75–85.
33. Fisher M (1963) *The Sea, Volume 2: The Composition of Sea-Water Comparative and Descriptive Oceanography* (Harvard Univ Press, Cambridge, MA).
34. Park JD, Cherrington NJ, Klaassen CD (2002) Intestinal absorption of cadmium is associated with divalent metal transporter 1 in rats. *Toxicol Sci* 68(2):288–294.
35. Yang H, Shu Y (2015) Cadmium transporters in the kidney and cadmium-induced nephrotoxicity. *Int J Mol Sci* 16(1):1484–1494.
36. Hinkle PM, Shanshala ED, 2nd, Nelson EJ (1992) Measurement of intracellular cadmium with fluorescent dyes. Further evidence for the role of calcium channels in cadmium uptake. *J Biol Chem* 267(35):25553–25559.
37. Grynkiewicz G, Poenie M, Tsien RY (1985) A new generation of Ca2+ indicators with greatly improved fluorescence properties. *J Biol Chem* 260(6):3440–3450.
38. Mayaan E, Moser A, MacKerell AD, Jr, York DM (2007) CHARMM force field parameters for simulation of reactive intermediates in native and thio-substituted ribozymes. *J Comput Chem* 28(2):495–507.
39. Zhu X, Lopes PEM, Mackerell AD, Jr (2012) Recent developments and applications of the CHARMM force fields. *Wiley Interdiscip Rev Comput Mol Sci* 2(1):167–185.
40. Autenrieth F, Tajkhorshid E, Baudry J, Luthey-Schulten Z (2004) Classical force field parameters for the heme prosthetic group of cytochrome c. *J Comput Chem* 25(13): 1613–1622.
41. Dal Peraro M, et al. (2007) Modeling the charge distribution at metal sites in proteins for molecular dynamics simulations. *J Struct Biol* 157(3):444–453.
42. Granata D, Camilloni C, Vendruscolo M, Laio A (2013) Characterization of the free-energy landscapes of proteins by NMR-guided metadynamics. *Proc Natl Acad Sci USA* 110(17):6817–6822.
43. Fiorin G, Klein ML, Henin J (2013) Using collective variables to drive molecular dynamics simulations. *Mol Phys* 111(22-23):3345–3362.
44. Martin JE, Waters LS, Storz G, Imlay JA (2015) The Escherichia coli small protein MntS and exporter MntP optimize the intracellular concentration of manganese. *PLoS Genet* 11(3):e1004977.
45. Jo S, Kim T, Iyer VG, Im W (2008) CHARMM-GUI: A web-based graphical user interface for CHARMM. *J Comput Chem* 29(11):1859–1865.
46. Ash WL, Zlomislic MR, Oloo EO, Tieleman DP (2004) Computer simulations of membrane proteins. *Biochim Biophys Acta* 1666(1-2):158–189.
47. Klauda JB, et al. (2010) Update of the CHARMM all-atom additive force field for lipids: Validation on six lipid types. *J Phys Chem B* 114(23):7830–7843.
48. Jorgensen WL, Chandrasekhar J, Madura JD, Impey RW, Klein ML (1983) Comparison of simple potential functions for simulating liquid water. *J Chem Phys* 79(2):926–935.
49. Duarte F, et al. (2014) Force field independent metal parameters using a nonbonded dummy model. *J Phys Chem B* 118(16):4351–4362.
50. LeBard DN, Martin DR, Lin S, Woodbury NW, Matyushov DV (2013) Protein dynamics to optimize and control bacterial photosynthesis. *Chem Sci (Camb)* 4(11):4127–4136.
51. Moin ST, Hofer TS, Sattar R, Ul-Haq Z (2011) Molecular dynamics simulation of mammalian 15S-lipoxygenase with AMBER force field. *Eur Biophys J* 40(6):715–726.
52. Spiegel K, De Grado WF, Klein ML (2006) Structural and dynamical properties of manganese catalase and the synthetic protein DF1 and their implication for reactivity from classical molecular dynamics calculations. *Proteins* 65(2):317–330.
53. Moradi M, Sagui C, Roland C (2014) Investigating rare events with nonequilibrium work measurements. II. Transition and reaction rates. *J Chem Phys* 140(3):034115.